

## Article

# A Multi-Cavity Iterative Modeling Method for the Exhaust Systems of Altitude Ground Test Facilities

Keqiang Miao<sup>1</sup>, Xi Wang<sup>1</sup>, Meiyin Zhu<sup>2,\*</sup> , Song Zhang<sup>3</sup>, Zhihong Dan<sup>3</sup>, Jiashuai Liu<sup>1</sup>, Shubo Yang<sup>1</sup>, Xitong Pei<sup>4</sup>, Xin Wang<sup>3</sup> and Louyue Zhang<sup>1</sup>

<sup>1</sup> School of Energy and Power Engineering, Beihang University, Beijing 100191, China; kqmiao@buaa.edu.cn (K.M.); xwang@buaa.edu.cn (X.W.); ljsbuaa@buaa.edu.cn (J.L.); yangshubo@buaa.edu.cn (S.Y.); sy2004112@buaa.edu.cn (L.Z.)

<sup>2</sup> Beihang Hangzhou Innovation Institute Yuhang, Hangzhou 310023, China

<sup>3</sup> Science and Technology on Altitude Simulation Laboratory, AECC Sichuan Gas Turbine Establishment, Mianyang 621703, China; goom2619@163.com (S.Z.); dzh798318\_cym@163.com (Z.D.); tywangxin2012@163.com (X.W.)

<sup>4</sup> Research Institute of Aero-Engine, Beihang University, Beijing 100191, China; peixitong@buaa.edu.cn

\* Correspondence: mecalzmy@buaa.edu.cn

**Abstract:** To solve the modeling problem of altitude ground test facility (AGTF) exhaust systems, which is caused by nonlinearity along the gas path and the difficulty of ejection factor calculation, a multi-cavity iterative modeling method is presented. The components of exhaust systems, such as the exhaust diffuser and cooler, are built with a series of volumes. It overcomes the disadvantage that traditional lumped-parameter models have, whereby they cannot calculate the dynamic parameters along the gas path. The exhaust system model is built with an iterative method based on multi-cavity components, and simulations are carried out under experimental conditions. The simulation results show that the maximum error of pressure is 2 kPa in the steady state and less than 6 kPa in the transient process compared with experimental data. Closed-loop simulations are also carried out to further verify the accuracy and effectiveness of the multi-cavity iterative exhaust system modeling method.

**Keywords:** altitude ground test facility; exhaust system; multi-cavity iterative model



**Citation:** Miao, K.; Wang, X.; Zhu, M.; Zhang, S.; Dan, Z.; Liu, J.; Yang, S.; Pei, X.; Wang, X.; Zhang, L. A Multi-Cavity Iterative Modeling Method for the Exhaust Systems of Altitude Ground Test Facilities. *Symmetry* **2022**, *14*, 1399. <https://doi.org/10.3390/sym14071399>

Academic Editor: Toshio Tagawa

Received: 5 June 2022

Accepted: 5 July 2022

Published: 7 July 2022

**Publisher's Note:** MDPI stays neutral with regard to jurisdictional claims in published maps and institutional affiliations.



**Copyright:** © 2022 by the authors. Licensee MDPI, Basel, Switzerland. This article is an open access article distributed under the terms and conditions of the Creative Commons Attribution (CC BY) license (<https://creativecommons.org/licenses/by/4.0/>).

## 1. Introduction

Altitude ground test facilities (AGTFs) can test the performances of aero engines over the flight envelope on the ground by simulating the inlet and outlet environment conditions of aero engines [1]. In order to reduce energy consumption in altitude ground test experiments with the aim of energy conservation and reducing expenses, the modeling of AGTFs has been a hot issue over the last decades. Moreover, the demand of the precise modeling of AGTF to design an advanced control algorithm with the purpose of realizing full mission profile flight trajectory continuous simulations for aero engines has been increasing for many years [2]. The exhaust system is an important component of AGTFs that is responsible for simulating air conditions after the engine nozzle. The modeling problem of the exhaust system results from the nonlinearity of components [3], especially the exhaust diffuser, which cools the gas exiting the engine nozzle by mixing it with air ejected from the test chamber and increases the static pressure of the mixed gas at the same time. The traditional lumped-parameter modeling method is insufficient to reflect the coupled dynamic of temperature and pressure inside. Moreover, due to the distance between the engine nozzle and the exhaust diffuser, the traditional method [4] cannot calculate the ejected secondary flow effectively. Research on exhaust diffuser simulations can be simplified with no induced secondary flow [5].

At the system level, the Arnold Engineering Development Complex (AEDC), which is located in America, has been conducting research on AGTF modeling and has been

updating simulation software since 2000 [6–8]. A mathematical model of an AGTF in Canada was built by Boraira in 2006 [9]. In Germany, a digital simulation platform was built by Bierkamp et al. [10] and was developed to a semi-physical simulation platform by Weisser in 2013 [11]. In China, a system-level model of AGTF was established by Pei et al. in 2019 [12].

At present, the majority of research on AGTF modeling focuses on the lumped-parameter method. In the platform built by Pei et al. in reference [12], the exhaust system of an AGTF is considered single volume, which sacrifices the accuracy of the exhaust system model. Many algorithms are presented to compensate system simulation results by improving the accuracy of components. Zhu et al. proposed a coordinate positioning and regression algorithm to improve the accuracy of butterfly valves in exhaust systems [13]. Sosunov considered the thermal inertia of pipes and proposed an unsteady temperature calculation method [14]. In 2022, Liu et al. started to focus on the axial dynamic performance in AGTFs and built a quasi-one-dimensional flow model of a pipe [15] because Sheeley et al. proved that the accuracy of the lumped-parameter model is inadequate [16]. Moreover, robust control algorithms such as scheduled proportional–integral control [17], linear active disturbance rejection [18] and  $\mu$  synthesis [19] are presented as a compromise to the inaccurate system model. It limits the development of the advanced control method, which maximizes the ability of AGTFs for more complicated experiments.

It can be concluded that there are increasing demands for an accurate model of exhaust systems that reflects the dynamic of the parameters along the symmetry components of the system. Therefore, a multi-cavity iterative modeling method for the exhaust systems of ATGFs is proposed in this paper. It separates exhaust systems into a series of volumes and calculates the parameters in each volume with the lumped-parameter method, because the exhaust system is composed of symmetry components, which means that the dynamic in the circumferential direction can be ignored. The dynamic of parameters in the axial direction can be reflected with lumped parameters in the ordered volumes. Moreover, the multi-cavity iterative modeling method introduces the initial guess values to ensure the smooth calculation of parameters. The iterative method takes the exhaust system as a whole and updates a series of system states at the same time, which increases the convergence of the model and speeds up the simulation process appropriately.

This paper is organized as follows. In Section 2, the multi-cavity components of the exhaust system are built. In Section 3, the exhaust system is built with a component model. The actual states of the system are achieved by solving residual differential equations with the Newton–Raphson iterative method. In Section 4, a simulation under different flight conditions is carried out, and the simulation results are compared with experimental data. Moreover, the simulation results are compared with the lumped-parameter model. Finally, conclusions are given in Section 5.

## 2. Component Model of the Exhaust System

The exhaust system is composed of a test chamber, exhaust diffuser, cooler, butterfly valves and pipe volume. Its structure is shown in Figure 1. The boundary conditions of the exhaust system consist of environment conditions, engine outlet conditions and Valve 3 outlet pressure conditions provided with the air extraction system. The environment condition includes temperature and pressure before Valve 1 and Valve 2. Since the outlet of the engine cannot be measured with sensors in the experiment directly, the mass flow, temperature, pressure and velocity, after the aero engine, are calculated with the inlet condition and states of aero engine, which consist of inlet mass  $W_0$ , inlet total temperature  $T_0$ , inlet total pressure  $P_0$ , power level angle (PLA), etc.

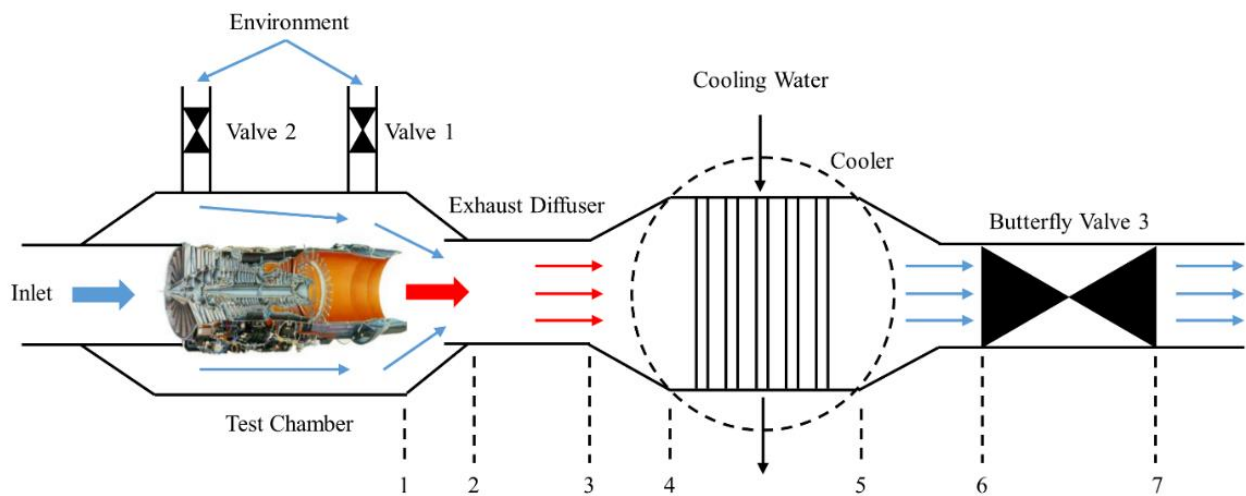


**Figure 1.** Structure of exhaust system.

The working medium in the exhaust system is a real gas that consists of the gas from the engine nozzle and air in the test chamber. However, because the pressure in the exhaust system is much lower than the atmospheric pressure (101 kPa) and the temperature is higher than 288.15 K, it is also reasonable to treat it as an ideal gas.

The units of the variables used in the modeling process are shown in Table 1.

**Table 1.** The units of variables.

Variable	Meaning	Units
$p$	Pressure	Pa
$T$	Temperature	K
$A$	Area	$m^2$
$d$	Diameter	m
$V$	Volume	$m^3$
$v$	Velocity	m/s
$W$	Mass flow	kg/s
$m$	Mass	kg
$c$	Specific heat	$J/(kg^{\circ}C)$
$R$	Gas constant	$J/(kg^{\circ}C)$
$h_t$	Unit enthalpy	J/kg
$h$	Heat transfer coefficient	$W/(m^2^{\circ}C)$
$E$	Energy	J
$U$	Internal energy	J
$\dot{Q}$	Heat transfer rate	J/s

### 2.1. Exhaust Diffuser Model

The exhaust diffuser is used to reduce the temperature and velocity of the high-temperature and high-speed gas discharged from engine nozzle. Moreover, it reduces the load of the air extraction system by increasing the static pressure of the gas.

The exhaust diffuser model built with the multi-cavity method is divided into three parts, which are the ejection model, mixture model and expansion model, and into four sections, which are boundaries of the three models and are shown in Figure 2.

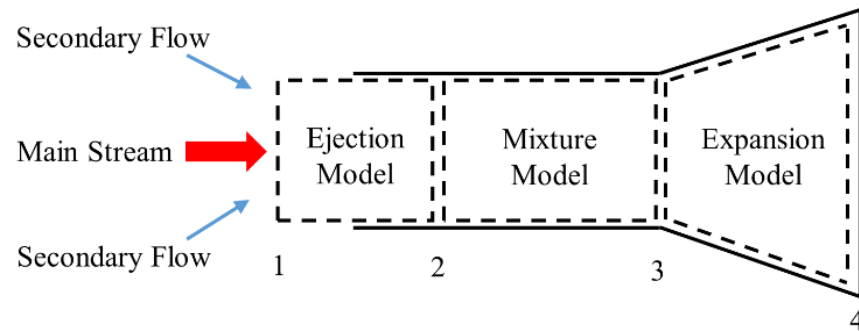


**Figure 2.** Multi-cavity exhaust diffuser model.

First, some theorems of aerodynamics need to be introduced.

**Theorem 1.** Aerodynamic function  $\pi(\lambda)$  describes the relationship between the static pressure  $p$  and the total pressure  $p_t$ . Moreover, it can be calculated with the specific heat ratio  $k$  and the velocity coefficient  $\lambda$  shown in Equation (1) [20].

$$\pi(\lambda) = \frac{p}{p_t} = \left(1 - \frac{k-1}{k+1}\lambda^2\right)^{\frac{k}{k-1}} \quad (1)$$

where, in  $\lambda = \frac{v}{v_{cr}}$ ,  $v$  is the velocity of gas and  $v_{cr}$  is critical acoustic velocity.

**Theorem 2.** The flow formula in Equation (2) describes the relationship between the mass flow  $W$  and the total parameters of the gas [20].

$$W = K \frac{p_t}{\sqrt{T_t}} A q(\lambda) \quad (2)$$

where  $K = \sqrt{\frac{k}{R} \left(\frac{2}{k+1}\right)^{\frac{k+1}{k-1}}}$  is calculated with the specific heat ratio  $k$  and gas constant  $R$ , and the flow function  $q(\lambda) = \left(\frac{k+1}{2}\right)^{\frac{1}{k-1}} \lambda \left(1 - \frac{k-1}{k+1}\lambda^2\right)^{\frac{1}{k-1}}$  is calculated with the specific heat ratio  $k$  and the velocity coefficient  $\lambda$ .  $p_t$  is the gas total pressure,  $T_t$  is the gas total temperature and  $A$  is the flow area.

**Theorem 3.** The impulse of a gas can be calculated with the mass flow, velocity, static pressure, flow area or total pressure, flow area, and flow function  $f(\lambda)$ . They are equal to each other, which is shown in Equation (3) [20].

$$WV + pA = p_t A f(\lambda) \quad (3)$$

where  $f(\lambda) = \left(\frac{2}{k+1}\right)^{\frac{1}{k-1}} q(\lambda)z(\lambda)$  and  $z(\lambda) = \frac{1}{\lambda} + \lambda$ .

Secondly, initial guess values need to be introduced into the calculation process of the exhaust diffuser model. They are listed in Table 2.

**Table 2.** The initial guess values of exhaust diffuser model.

Variable	Meaning
$u$	Ejection factor
$P_{s2}$	Static pressure at Section 2
$P_{t3}$	Total pressure at Section 3
$\lambda_4$	Velocity coefficient at Section 4

Then, the calculation process from Sections 1–4 is shown as follows.

### 2.1.1. Ejection Model

In the ejection process, the main stream expands slightly and increases the speed of the secondary flow in the ejection model shown in Figure 3. The ejection model calculates the mass of the secondary flow  $W_{1s}$  with the mass of the main stream  $W_{1m}$  and the ejection factor  $u$ , as shown in Equation (4). The flow area of the main stream and the secondary flow at Section 2, which are denoted as  $A_{2m}$  and  $A_{2s}$ , are also obtained.

$$W_{1s} = uW_{1m} \tag{4}$$

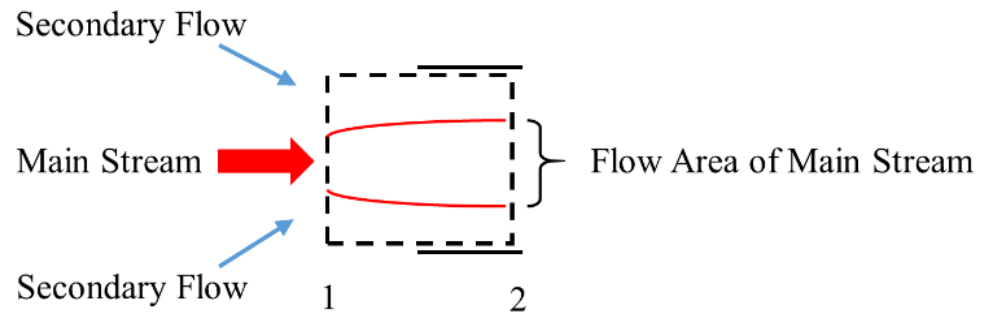


Figure 3. Diagram of ejection model.

The total pressure and total temperature of the main stream and secondary flow from Sections 1 and 2 are invariable because it is an isentropic expansion process. It is denoted as

$$p_{t2m} = p_{t1m}, p_{t2s} = p_{t1s} \tag{5}$$

$$T_{t2m} = T_{t1m}, T_{t2s} = T_{t1s} \tag{6}$$

where  $p_{t1m}$  is the total pressure of the main stream at Section 1 and  $p_{t2m}$  is the total pressure of the main stream at Section 2.  $T_{t1m}$  is the total temperature of the main stream at Section 1, and  $T_{t2m}$  is the total temperature of the main stream at Section 2.  $p_{t1s}$  is the total pressure of the secondary flow at Section 1, and  $p_{t2s}$  is the total pressure of the secondary flow at Section 2.  $T_{t1s}$  is the total temperature of the secondary flow at Section 1, and  $T_{t2s}$  is the total temperature of the secondary flow at Section 2.

Then,  $\pi(\lambda)$  of the main stream at Section 2 can be calculated with the total pressure  $P_{s2m}$  and the initial guess value  $P_{s2}$ .

$$\pi(\lambda_{2m}) = \frac{P_{s2}}{p_{t2m}} \tag{7}$$

The velocity coefficient of the main stream can be obtained with the inverse function in Theorem 1. It is denoted as

$$\lambda_{2m} = \pi^{-1}(\lambda_{2m}) \tag{8}$$

Then,  $q(\lambda)$  of the main stream at Section 2 can be obtained with

$$q(\lambda_{2m}) = \left(\frac{k+1}{2}\right)^{\frac{1}{k-1}} \lambda_{2m} \left(1 - \frac{k-1}{k+1} \lambda_{2m}^2\right)^{\frac{1}{k-1}} \tag{9}$$

Moreover, because of the flow conservation law, we have

$$W_{2m} = W_{1m} \tag{10}$$

$$W_{2s} = W_{1s} \tag{11}$$

The equivalent flow area of the main stream at Section 2 is defined as

$$A_{2m} = \frac{q(\lambda_{1m})}{q(\lambda_{2m})} A_{1m} \quad (12)$$

where  $A_{1m}$  is the output area of the engine.

Then, the equivalent flow area of secondary flow at Section 2 is defined as

$$A_{2s} = \frac{\pi d^2}{4} - A_{2m} \quad (13)$$

where  $d$  is the diameter of the exhaust diffuser.

### 2.1.2. Mixture Model

The mixture model calculates the temperature and pressure of the well-mixed gas by mixing the main stream and secondary flow at Section 2, as shown in Figure 4. The mixing process should meet the laws of flow conservation, energy conservation, impulse conservation and pressure balance.

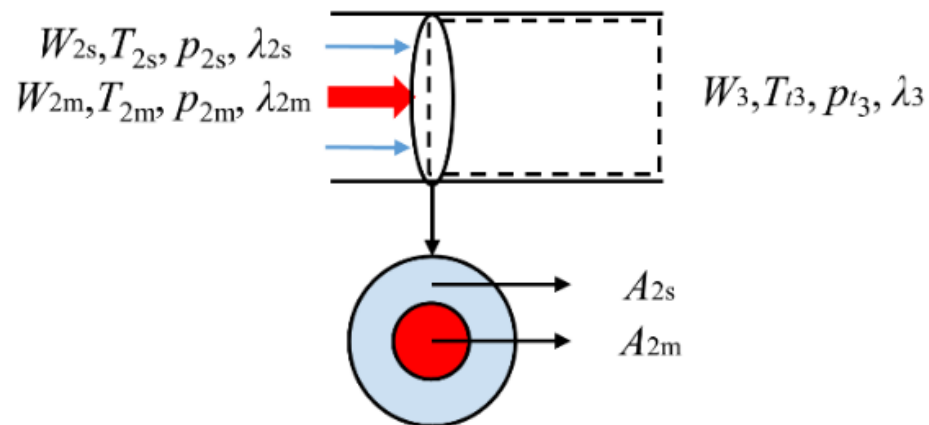


**Figure 4.** Diagram of mixture model.

The velocity coefficient  $\lambda_{2s}$  can be obtained with Theorem 2 because  $W_{2s}$ ,  $T_{t2s}$ ,  $P_{t2s}$  and  $A_{2s}$  are obtained from Equations (5), (6), (11) and (13). Then,  $\pi(\lambda_{2s})$  can be obtained with Theorem 1.

The static pressure of the secondary flow at Section 2 can be calculated with  $\pi(\lambda)$  in Equation (14).

$$p_{s2s} = p_{t2s} \pi(\lambda_{2s}) \quad (14)$$

The static pressure of the main stream and secondary flow should be balanced at Section 2. This means that  $p_{s2m} = p_{s2s}$ . The relative error of the static pressure at Section 2 is denoted with

$$e_1 = (p_{s2s} - p_{s2m}) / p_{s2m} \quad (15)$$

The calculation process of static pressure balance, including Equations (7)–(15), is shown in Figure 5.

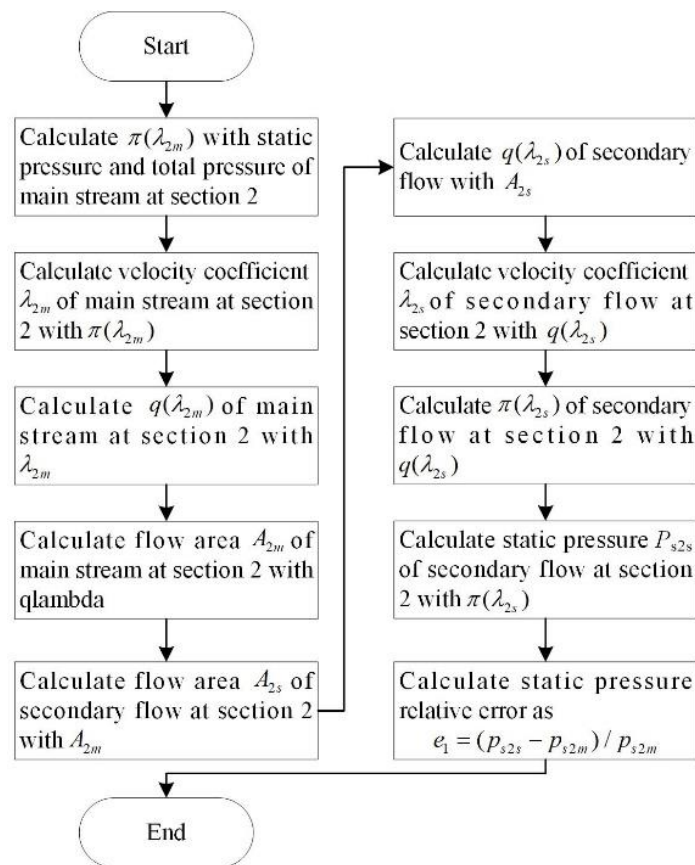


Figure 5. Calculation process of static pressure balance at Section 2.

The unit enthalpy at Section 3 can be calculated with the energy conservation law, as shown in Equation (16). The temperature is obtained with Equation (17).

$$h_{t3} = (h_{t2m}W_{2m} + h_{t2s}W_{2s})/W_3 \quad (16)$$

$$T_{t3} = h_{t3}/C_p \quad (17)$$

where  $W_3 = W_{2s} + W_{2m}$ , and  $h_t$  is unit enthalpy at each section.

The impulse of the gas at Sections 2 and 3 can be obtained with the right part of Equation (3) in Theorem 3. Because the mass flow at Sections 2 and 3 meets the impulse conservation law, we have

$$p_{t2m}A_{2m}f(\lambda_{2m}) + p_{t2s}A_{2s}f(\lambda_{2s}) = p_{t3}A_3f(\lambda_3) \quad (18)$$

The relative error of impulse is denoted as

$$e_2 = (p_{t2m}A_{2m}f(\lambda_{2m}) + p_{t2s}A_{2s}f(\lambda_{2s}) - p_{t3}A_3f(\lambda_3)) / (p_{t2m}A_{2m}f(\lambda_{2m}) + p_{t2s}A_{2s}f(\lambda_{2s})) \quad (19)$$

### 2.1.3. Expansion Model

The inputs and outputs of the expansion model are shown in Figure 6. It is assumed that the process between Sections 3 and 4 is isentropic and adiabatic. Therefore, the total temperature and total pressure can be obtained with

$$p_{t4} = p_{t3} \quad (20)$$

$$T_{t4} = T_{t3} \quad (21)$$

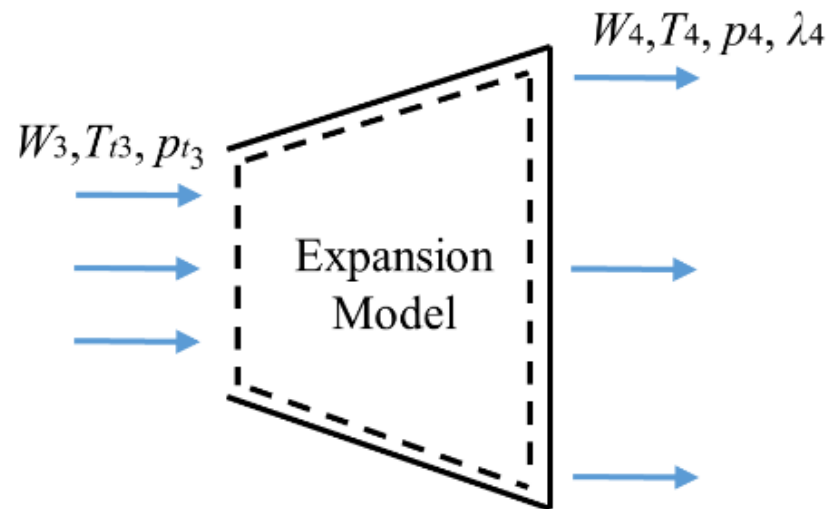


Figure 6. Diagram of expansion model.

Then, the mass flow at Section 4 can be calculated with Theorem 3 as

$$W_4 = K \frac{p_{t4}}{\sqrt{T_{t4}}} A_4 q(\lambda_4) \quad (22)$$

where  $A_4 = \frac{\pi D^2}{4}$  is the exit area of the expansion stage.

As a result of flow conservation, we have  $W_4 = W_3$ . Then, the relative error of the mass flow is defined as

$$e_3 = (W_4 - W_3) / W_3 \quad (23)$$

The exit static pressure of the exhaust diffuser model is

$$p_4 = \pi(\lambda_4) p_{t4} = \left(1 - \frac{k-1}{k+1} \lambda_4^2\right)^{\frac{1}{k-1}} p_{t4} \quad (24)$$

The exit static temperature of the exhaust diffuser model is

$$T_4 = \tau(\lambda_4) T_{t4} = \left(1 - \frac{k-1}{k+1} \lambda_4^2\right) T_{t4} \quad (25)$$

## 2.2. Cooler Model

In the exhaust system, the cooler improves the gas flow capacity and reduces the aging of the equipment by reducing the gas temperature. The high-temperature gas passing through the cooling pipes with the cooling water inside is cooled to the allowable working temperature. The structure of the cooler in the exhaust system is shown in Figure 7. It is divided into  $n$  volumes, and it is assumed that the temperature in each volume between pipes is even. Then, the temperature decreases gradually from  $T_{v,1}$  to  $T_{v,n}$  in the volumes.

The heat transfer process of each pipe is shown in Figure 8. The heat transfers from the gas to the pipe and then to the cooling water. Finally, the heat is brought out of the system by the cooling water. The heat transfer rate between the gas and the pipe is denoted as

$$\dot{Q}_1 = h_1 A_1 (T_1 - T_m) \quad (26)$$

where  $h_1$  is heat transfer coefficient between the gas and the pipe,  $A_1$  is the contact area,  $T_1$  is the average temperature of gas and  $T_m$  is the average temperature of the pipe.

The heat transfer rate between the water and the pipe is denoted as

$$\dot{Q}_2 = h_2 A_2 (T_2 - T_m) \quad (27)$$

where  $h_2$  is heat transfer coefficient between the gas and the pipe,  $A_2$  is the contact area,  $T_2$  is the average temperature of cooling water and  $T_m$  is the average temperature of the pipe.

The heat quantity brought out of the system by the cooling water is

$$\dot{Q}_3 = W_2 C_{p2} (T_2 - T_{2in}) \quad (28)$$

where  $W_2$  is the mass of the cooling water in each pipe,  $C_{p2}$  is the specific heat of the cooling water,  $T_2$  is the average temperature of the cooling water and  $T_{2in}$  is the original temperature of the cooling water.

Therefore, the energy change rate of the pipe is

$$\frac{dE_m}{dt} = \dot{Q}_1 + \dot{Q}_2 \quad (29)$$

Moreover, the energy of the pipe can be defined as

$$E_m = c_m m_m T_m \quad (30)$$

where  $c_m$  is the specific heat of the pipe,  $m_m$  is the mass of the pipe and  $T_m$  is the average temperature of the pipe.

Another definition of the energy change rate of the pipe is shown in Equation (31), which is obtained by differentiating Equation (30).

$$\frac{dE_m}{dt} = c_m m_m \frac{dT_m}{dt} \quad (31)$$

The differential equation of the pipe temperature is obtained by substituting Equation (29) into Equation (31). It is denoted as

$$\frac{dT_m}{dt} = \frac{h_1 A_1 (T_1 - T_m) + h_2 A_2 (T_2 - T_m)}{c_m m_m} \quad (32)$$

With the same calculation, we can obtain the differential equation of the gas temperature and the differential equation of the water temperature, as shown in Equations (33) and (34). The output temperature of the gas  $T_{1out}$  and the output temperature of the cooling water  $T_{2out}$  are shown in Equations (35) and (36).

$$\frac{dT_1}{dt} = -\frac{h_1 A_1 (T_1 - T_m)}{c_{p1} W_1} \quad (33)$$

$$\frac{dT_2}{dt} = \frac{-h_2 A_2 (T_2 - T_m) - W_2 C_{p2} (T_2 - T_{2in})}{c_{p2} W_2} \quad (34)$$

$$T_{1out} = T_1 + \frac{dT_1}{dt} \quad (35)$$

$$T_{2out} = T_{2in} + \frac{dT_2}{dt} \quad (36)$$

where  $c_{p1}$  is the specific heat of the gas, and  $W_1$  is the mass of the gas flow through a pipe.

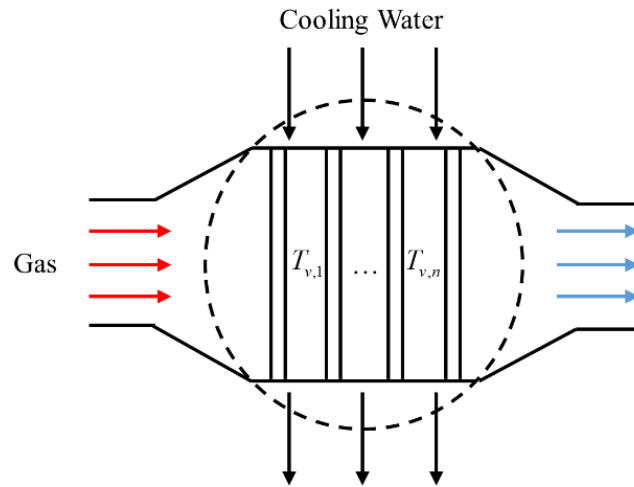


Figure 7. Structure of cooler.

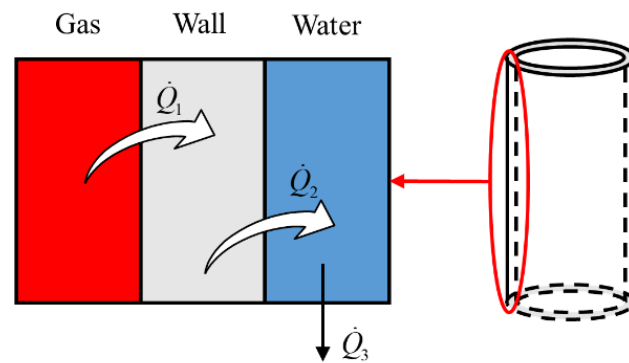


Figure 8. Diagram of cooling pipe heat transfer.

### 2.3. Butterfly Valve Model

A butterfly valve is used to regulate the pressure in the test chamber by controlling the mass flow exiting the exhaust system. The mass passing the butterfly valve depends on the pressure and temperature before the valve, the pressure after the valve and the opening of the valve. The structure of butterfly is shown in Figure 9.

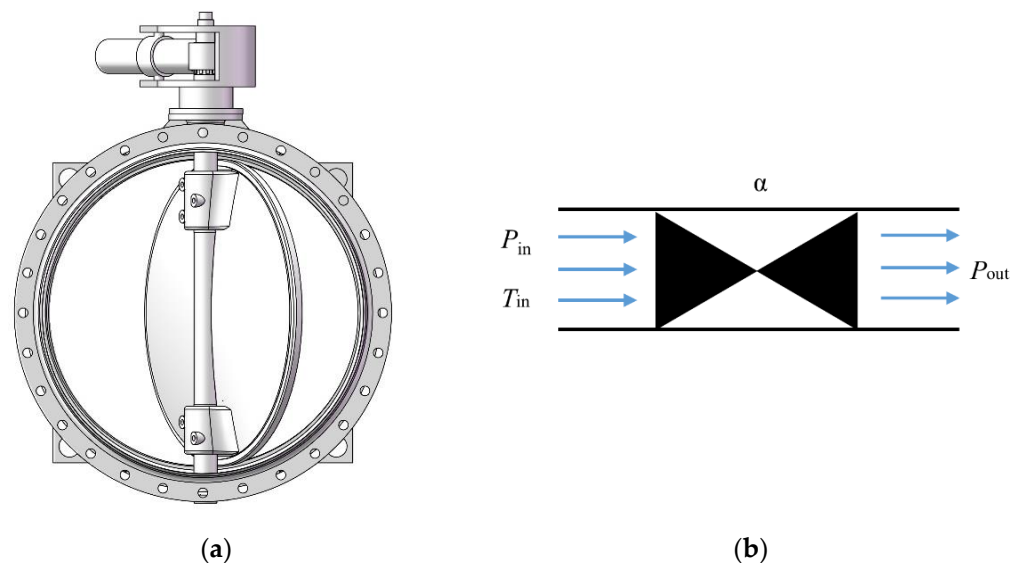
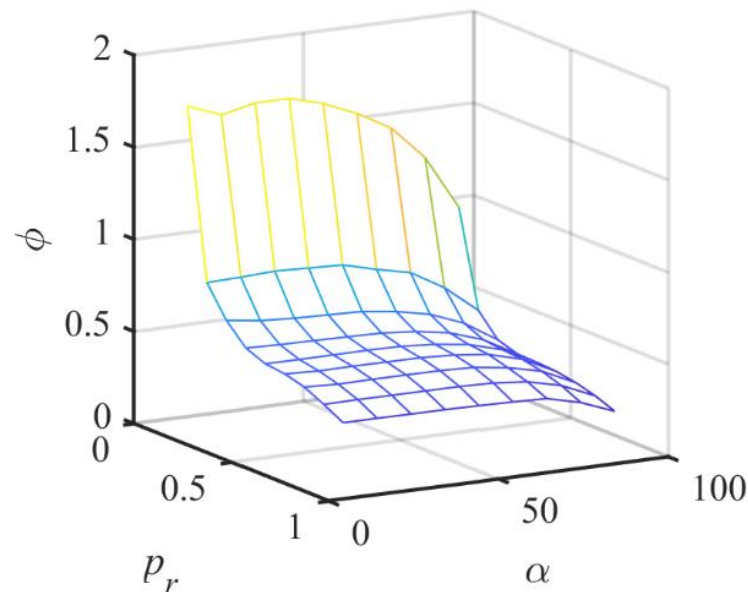


Figure 9. Model of butterfly valve: (a) Structure of butterfly valve; (b) Diagram of butterfly valve.

The butterfly valve is modeled in the form of a flow characteristic model with a flow coefficient map, as shown in Figure 10, and the flow function is denoted in Equation (37).

$$W = \phi \frac{\pi D^2}{4} \left(1 - \cos \frac{\alpha \pi}{180}\right) \cdot p_{in} \cdot \sqrt{\frac{2}{RT_{in}}} \quad (37)$$

where  $W$  is the mass flow through the valve, and  $D$  is the diameter of the valve. The flow coefficient  $\phi$  can be calculated with the valve pressure ratio  $p_r = \frac{p_{out}}{p_{in}}$  and the valve opening  $\alpha$ .



**Figure 10.** Flow coefficient map of butterfly valve.

#### 2.4. Test Chamber Model and Pipe Volume Model

The test chamber is the test section of the exhaust system that simulates the exhaust environment of the engine at a high altitude by controlling the mass of the entering flow and exiting flow. The entering flow is controlled with Valve 1 and Valve 2 in this test chamber, which is the valve flow in Figure 11. The exiting flow is ejected by the engine exhaust gas, which is the secondary flow in Figure 11.

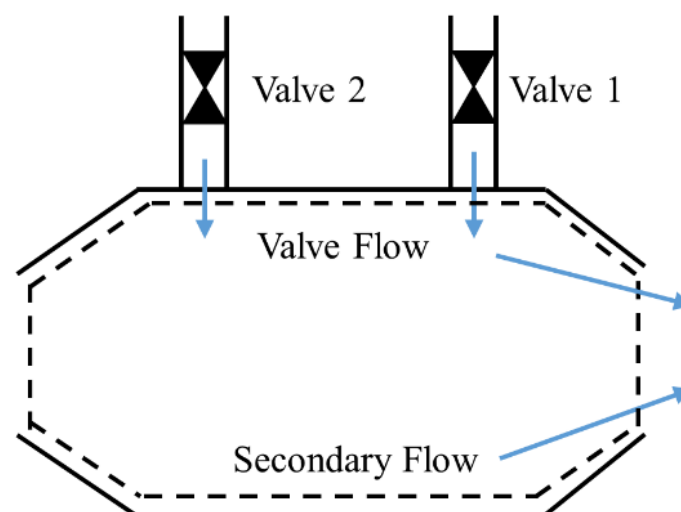


**Figure 11.** Structure of test chamber.

The internal energy equation of the air in the test chamber is defined as

$$U = WC_vT = W(C_p - R)T \quad (38)$$

where  $U$  is the internal energy of the air in the test chamber,  $W$  is the mass of the air in the test chamber,  $T$  is the temperature of the air in the test chamber,  $R$  is the gas constant,  $C_v$  is the specific heat of the gas at a constant volume and  $C_p$  is the specific heat of the gas at a constant pressure.

The energy differential equation in Equation (39) is obtained by differentiating Equation (38).

$$\frac{dU}{dt} = \frac{dW}{dt}(C_p - R)T + W(C_p - R)\frac{dT}{dt} \quad (39)$$

Moreover, the energy differential equation in Equation (39) can be deduced from the law of energy conservation.

$$\frac{dE}{dt} = W_{in}\left(C_pT_{in} + \frac{v_{in}^2}{2}\right) - W_{out}\left(C_pT_{out} + \frac{v_{out}^2}{2}\right) \quad (40)$$

where  $E$  is energy of the air in the test chamber, and  $W_{in}$  is the mass of the air entering the test chamber, which is the valve flow.  $T_{in}$  is the temperature of the air entering the test chamber.  $v_{in}$  is the velocity of the air entering the test chamber and is calculated with the mass of the air and the inlet area of the test chamber.  $W_{out}$  is the mass of the air exiting the test chamber, which is the secondary flow.  $T_{out}$  is the temperature of the air exiting the test chamber.  $v_{out}$  is the velocity of the air exiting the test chamber and is calculated with the mass of the air and the exiting area of the test chamber.

It is assumed that the air in the test chamber does not exchange heat with the wall. Therefore,

$$\frac{dE}{dt} = \frac{dU}{dt} \quad (41)$$

The change in the mass is denoted as

$$\frac{dW}{dt} = W_{in} - W_{out} \quad (42)$$

The ideal gas equation of state is shown in Equation (43).

$$PV = WRT \quad (43)$$

The temperature differential equation of the air in the test chamber, as shown in Equation (44), can be deduced with Equations (39)–(43).

$$\frac{dT}{dt} = \frac{RT}{PV(C_p - R)} \left[ (C_p - R)T(W_{out} - W_{in}) + \left( C_pT_{in} + \frac{v_{in}^2}{2} \right) W_{in} - \left( C_pT_{out} + \frac{v_{out}^2}{2} \right) W_{out} \right] \quad (44)$$

The pressure differential equation of the ideal gas, as shown in Equation (45), can be obtained by differentiating the ideal gas equation of state in Equation (43).

$$\frac{dP}{dt} = \frac{RT}{V} \frac{dW}{dt} + \frac{P}{T} \frac{dT}{dt} \quad (45)$$

The pressure differential equation of the air in the test chamber, as shown in Equation (46), can be obtained by substituting Equations (43) and (44) into Equation (45).

$$\frac{dP}{dt} = \frac{R}{V(C_p - R)} \left[ \left( C_pT_{in} + \frac{v_{in}^2}{2} \right) W_{in} - \left( C_pT_{out} + \frac{v_{out}^2}{2} \right) W_{out} \right] \quad (46)$$

The pressure and temperature inside the test chamber at time  $t + \Delta t$  can be denoted with the pressure and temperature at time  $t$  and the variation within  $\Delta t$ .

$$P^+ = P + \frac{dP}{dt} \Delta t \quad (47)$$

$$T^+ = T + \frac{dT}{dt} \Delta t \quad (48)$$

The pipe volume model represents the pipe connecting the components above. In the exhaust system, it is the volume between the exhaust diffuser and Valve 3. It can be modeled the same as the test chamber model with one input and one output. However, the heat brought out of the volume by the cooler must be considered. Therefore, Equation (40) is augmented as Equation (49). The differential equations of temperature and pressure in Equations (44) and (46) are transformed into Equations (50) and (51). A diagram of the pipe volume model is shown in Figure 12.

$$\frac{dE}{dt} = W_{in} \left( C_p T_{in} + \frac{v_{in}^2}{2} \right) - W_{out} \left( C_p T_{out} + \frac{v_{out}^2}{2} \right) - \sum \dot{Q}_1 \quad (49)$$

where  $\sum \dot{Q}_1$  is the total heat quantity brought out of the gas in the cooler.

$$\frac{dT}{dt} = \frac{RT}{PV(C_p - R)} \left[ (C_p - R)T(W_{out} - W_{in}) + \left( C_p T_{in} + \frac{v_{in}^2}{2} \right) W_{in} - \left( C_p T_{out} + \frac{v_{out}^2}{2} \right) W_{out} + \sum \dot{Q}_1 \right] \quad (50)$$

$$\frac{dP}{dt} = \frac{R}{V(C_p - R)} \left[ \left( C_p T_{in} + \frac{v_{in}^2}{2} \right) W_{in} - \left( C_p T_{out} + \frac{v_{out}^2}{2} \right) W_{out} + \sum \dot{Q}_1 \right] \quad (51)$$

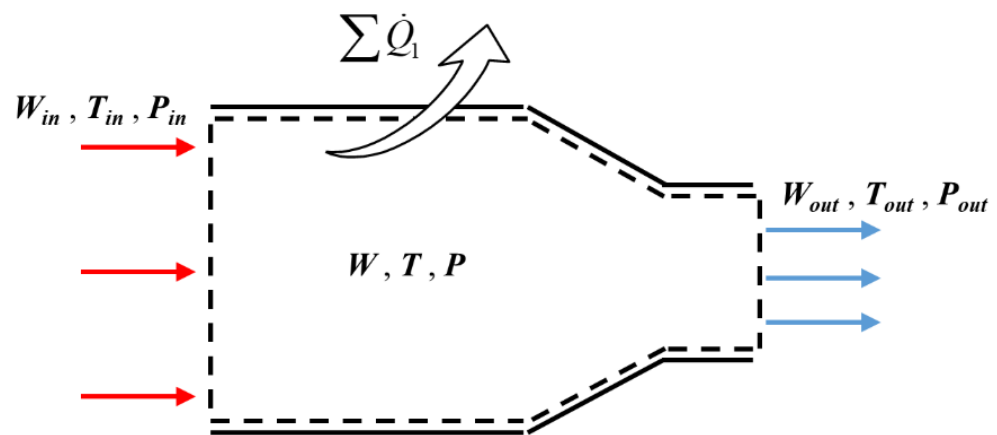


Figure 12. Diagram of pipe volume model.

### 3. Iterative Model of the Exhaust System

The exhaust system consists of two dynamic cavities whose temperature and pressure change when the flow balance of the inlet and outlet breaks. One of the cavities is the test chamber, and the other is the pipe volume. Since the main purpose of the exhaust system is to simulate the exhaust pressure of the engine, the pressure in the two dynamic cavities is chosen as the system states. The static pressure in the test chamber ( $p_{1s}$ ) is mainly decided by the valve flow passing through Valve 1 and Valve 2 and the secondary flow ejected by the engine. The static pressure in the pipe volume ( $p_5$ ) is mainly decided by the output mass of the exhaust diffuser and the mass passing through Valve 3.

In the calculation process of the exhaust diffuser, four initial guess values are introduced. This means that four residual equations are needed. By solving the residual equations with the iteration method, the initial guess values can be replaced with the true values of system gradually. The first three equations are shown in Equations (15), (19) and (23).

The fourth equation is the balance of the exhaust diffuser output pressure  $p_4$  and the pipe volume pressure  $p_5$ , as shown in Equation (52).

$$e_4 = (p_5 - p_4) / p_5 \tag{52}$$

The relationship between the components is shown in Figure 13. The inlet conditions, system states and control values of the exhaust system model are listed in Table 3.

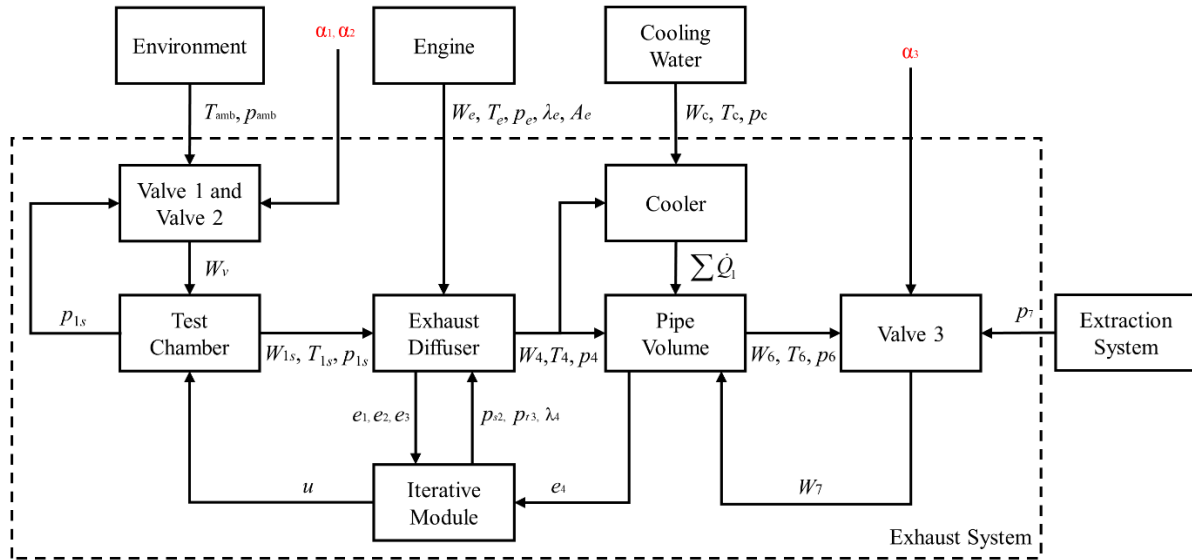


Figure 13. Logic diagram of exhaust system iterative model.

Table 3. Inlet conditions and control values of exhaust system model.

Type	Variable	Meaning
Inlet conditions	$p_{amb}$	Environment pressure
	$T_{amb}$	Environment temperature
	$W_e$	Mass flow of engine nozzle exit
	$T_e$	Temperature of engine nozzle exit
	$p_e$	Pressure of engine nozzle exit
	$\lambda_e$	Velocity coefficient of engine nozzle exit
	$A_e$	Flow area of engine nozzle exit
	$W_c$	Mass flow of cooling water
	$T_c$	Temperature of cooling water
	$p_c$	Pressure of cooling water
System states	$p_{1s}$	Static pressure in test chamber
	$p_6$	Static pressure in pipe volume
Control values	$\alpha_1$	Opening of Valve 1
	$\alpha_2$	Opening of Valve 2
	$\alpha_3$	Opening of Valve 3

#### 4. Model Simulation and Verification

In order to verify the accuracy of the exhaust system model, its simulation results should be compared with experimental data. The experimental data used in this paper were obtained in an experiment during the research of a turbofan engine at the AGTF of the AECC Sichuan Gas Turbine Establishment. It tests the performances of engines from idle to intermediate states at different flight heights, including 3 km, 5 km and 10 km. The experimental data were divided into four different types, which are mass flow, temperature, pressure and valve opening. They were obtained with four different kinds of sensors, which were orifice meters, temperature sensors, pressure sensors and linear displacement sensors.

As a result of the linear relationship between the displacement of the actuator and the opening of butterfly valve, as shown in Equation (53), the  $\alpha_1$ ,  $\alpha_2$  and  $\alpha_3$  could be calculated with the displacement measured with the linear displacement sensors. The arrangement of the sensors in the exhaust system is shown in Figure 14. Their manufacturers and accuracy are listed in Table 4. The measured experimental data are shown in Figure 15.

$$\alpha = \frac{90}{L_{\max}}L \quad (53)$$

where  $L_{\max}$  is the maximum stroke of the hydraulic cylinder, and  $L$  is the current displacement measured by the sensor.

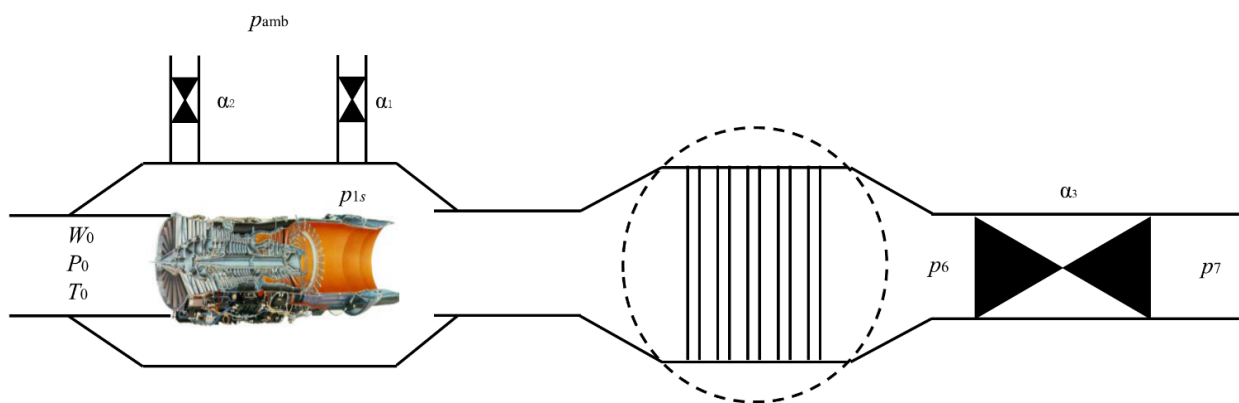


Figure 14. Arrangement of sensors.

Table 4. Type and accuracy of sensors.

Type	Manufacturer	Accuracy
Orifice meter	Chuanyi	$\pm 1\%$
Temperature sensor	Therncway	$\pm 0.5\%$
Pressure sensor	Honeywell	$\pm 0.1\%$
Linear displacement sensor	MTS	$\pm 0.1\%$

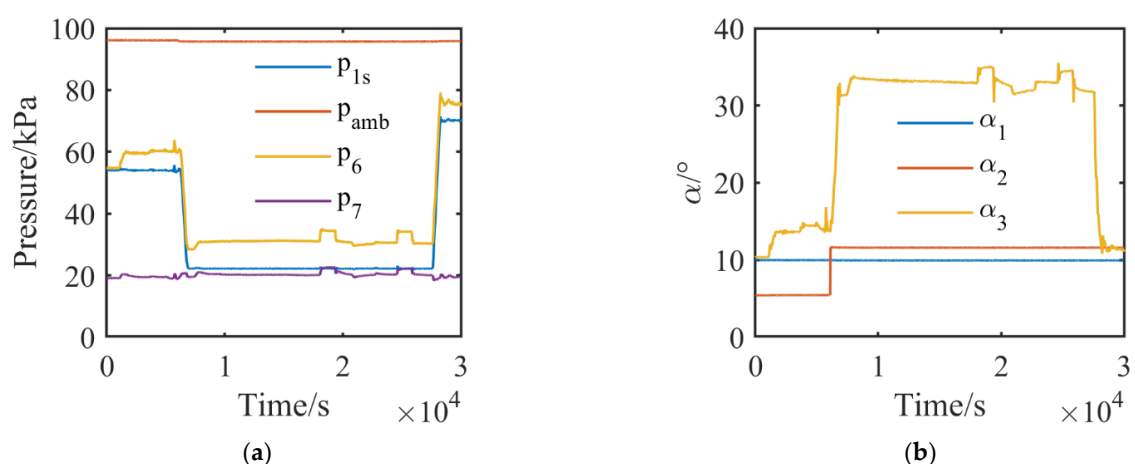
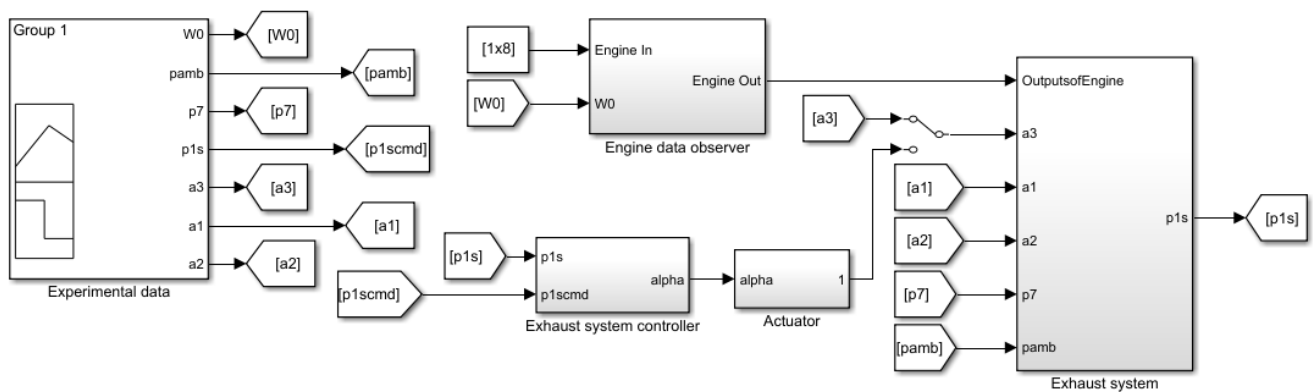


Figure 15. Experimental data: (a) Pressure of exhaust system; (b) Opening of valves in exhaust system.

#### 4.1. Model Verification with Experimental Data and Observed Engine Parameters

The exhaust system model was built with Matlab in Simulink. The simulation platform is shown in Figure 16. It consisted of the experimental data module, engine data observer module, exhaust system controller module, actuator module and exhaust system module.



**Figure 16.** Simulation platform for exhaust system validation.

The experimental data module contained the data that are shown in Figure 15. The engine data observer module calculated the outlet mass flow  $W_e$ , pressure  $P_e$ , temperature  $T_e$  and nozzle throat area  $A_e$  of the engine based on the states of the engine because they were not measured directly. They are shown in Figure 17. The controller and the actuator were used to test the performance of the exhaust system built with the multi-cavity method in a closed-loop system. It was a PI controller with  $P = 0.001$  and  $I = 0.1$ . The pressure in the test chamber was regulated to the desired value by adjusting the opening of Valve 3 with this PI controller by switching the manual switch module and activating the control loop. The transfer function of the valve actuator was assumed as  $\frac{1}{0.1s+1}$ .

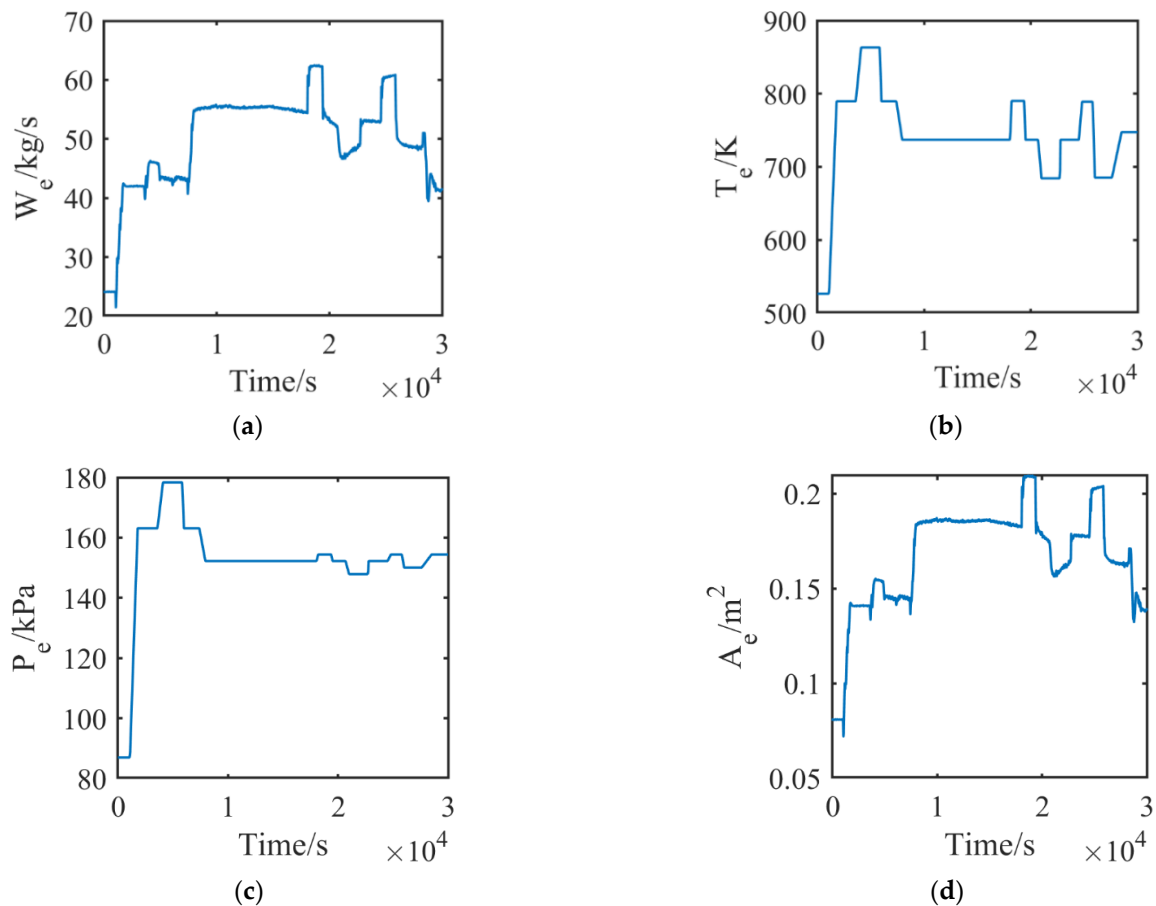


**Figure 17.** Observed engine parameters: (a) Mass flow of engine; (b) Total temperature after turbine; (c) Total pressure after turbine; (d) Throat area of engine nozzle.

The simulation platform was solved with the Heun method and a fixed step size of 0.01.

A simulation under the same working conditions as in the experiment was carried out. The inlet conditions and the control values of the exhaust system model that are shown in Table 2 were set with the experimental data module and the engine data observer module, as shown in Figure 16. Other parameters were set as constants. The temperature of the environment and cooling water was 288.15 K. The velocity coefficient  $\lambda_e$  at the nozzle throat was 1.

The simulation results compared with experimental data are shown in Figure 18. The pressure error between the simulation results and experimental data was no more than 2 kPa in the steady state and less than 6 kPa in the transient process.

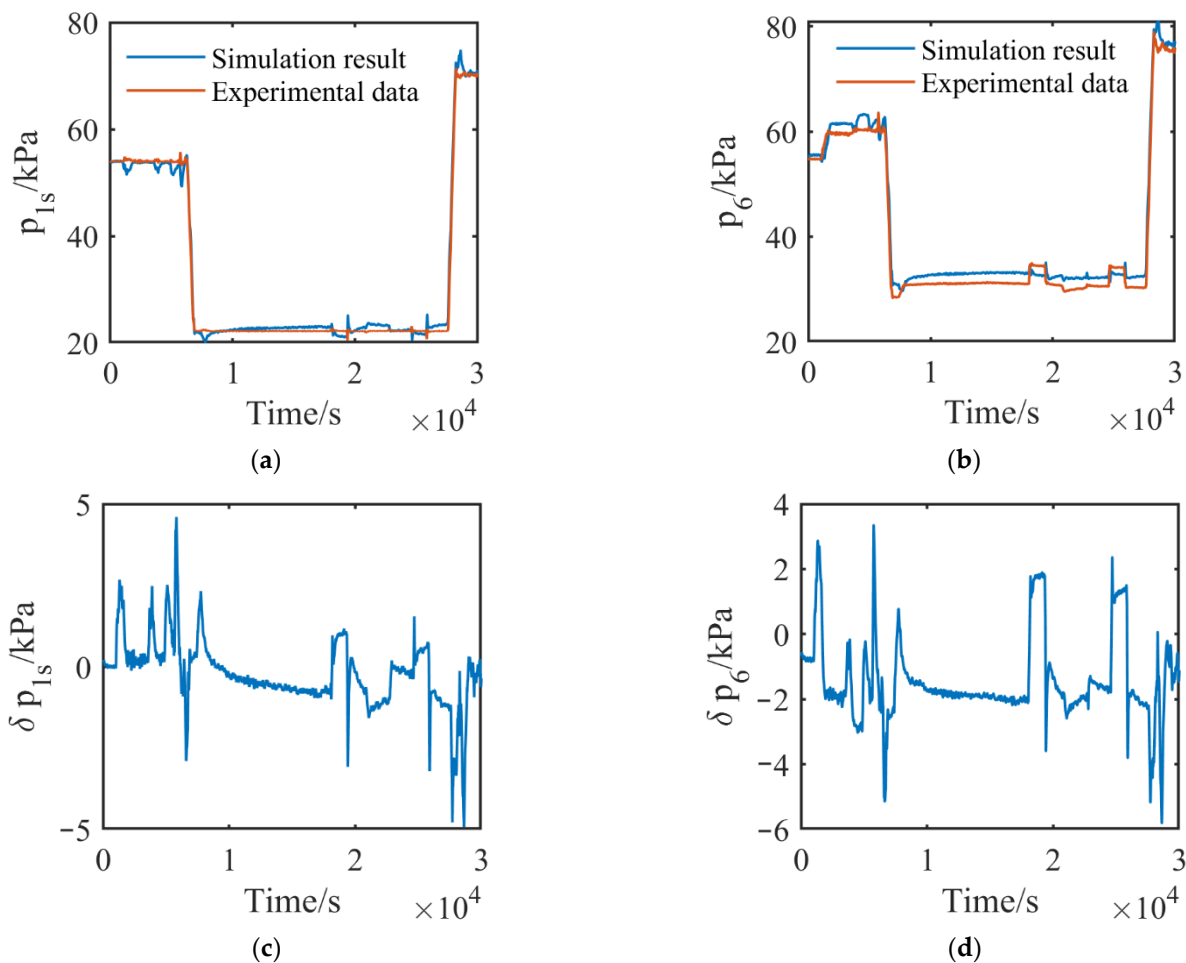


**Figure 18.** Simulation results of pressure: (a) Pressure in test chamber; (b) Pressure before Valve 3; (c) Error of pressure in test chamber; (d) Error of pressure before Valve 3.

#### 4.2. Simulation Results Compared with Lumped-Parameter Model

It should be known that, in the modeling procedure of the test chamber and pipe volume model, the the main reason for the pressure dynamic in the volume is the inflow and outflow mass. Therefore, the mass calculation becomes an important part of the exhaust system model for both accurate calculations and dynamic performance analysis.

The simulation results of mass are shown in Figure 19. Taking the exhaust system shown in Figure 13 as a whole, the total mass flow into the system consists of the valve flow  $W_v$ , which is the sum of the mass that passes through Valve 1 and Valve 2, and the engine flow  $W_e$ . The mass flow out of the system includes mass that passes through Valve 3, which is denoted as  $W_7$ . They are equal to each other in the steady state, and both of them increase and decrease with the engine state as the mass flow  $W_e$  changes. It should be mentioned

that  $W_7$  increases around time 6000 s and decreases around time 27,600 s quickly, as shown in Figure 19a. It results from rapid opening change of Valve 3, as shown in Figure 15b, with the purpose of changing the pressure  $p_{1s}$  in the test chamber, as shown in Figure 15a. The dynamic performance of the test chamber, as shown in Figure 11, is defined with the input denoted as valve flow  $W_v$  and the output denoted as secondary flow  $W_{1s}$ . It is shown in Figure 19b that the valve flow  $W_v$  equals the secondary flow  $W_{1s}$  in the steady state, and the balance is broken in the transient process of the engine or exhaust system.

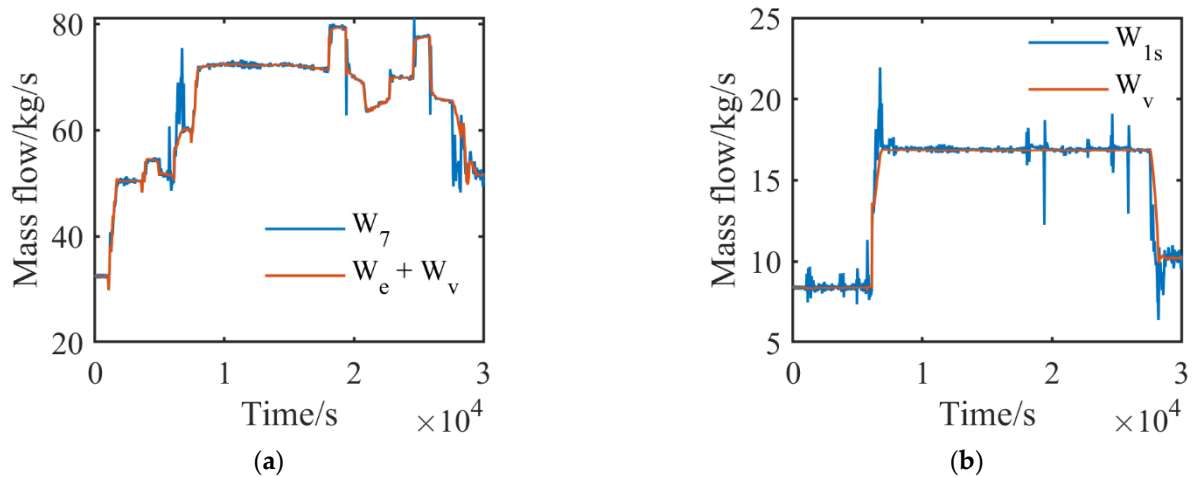


**Figure 19.** Simulation results of mass flow: (a) Mass flow of exhaust system; (b) Mass flow of test chamber.

The secondary flow of mass  $W_{1s}$ , which is ejected by the main stream of mass  $W_{1m}$  and defined in Equation (4), is the output of the test chamber model and one of inputs of the exhaust system volume. It is a bridge connecting the two main volumes, which is the test chamber and pipe volume, as shown in Figure 13, in the exhaust system. The multi-cavity iterative exhaust system model calculates secondary flow based on the exhaust parameters of the engine, the pressure in the test chamber and the pressure in the exhaust system by iteration. It makes the model have the advantage of calculating the pressure difference more accurately compared with the traditional lumped-parameter model. The lumped parameter model of AGTF exhaust systems was first proposed in reference [12], and its logic diagram is shown in Figure 20. It simplifies the exhaust system as a single volume without considering the pressure dynamic in the exhaust diffuser and the heat exchange in the cooler.

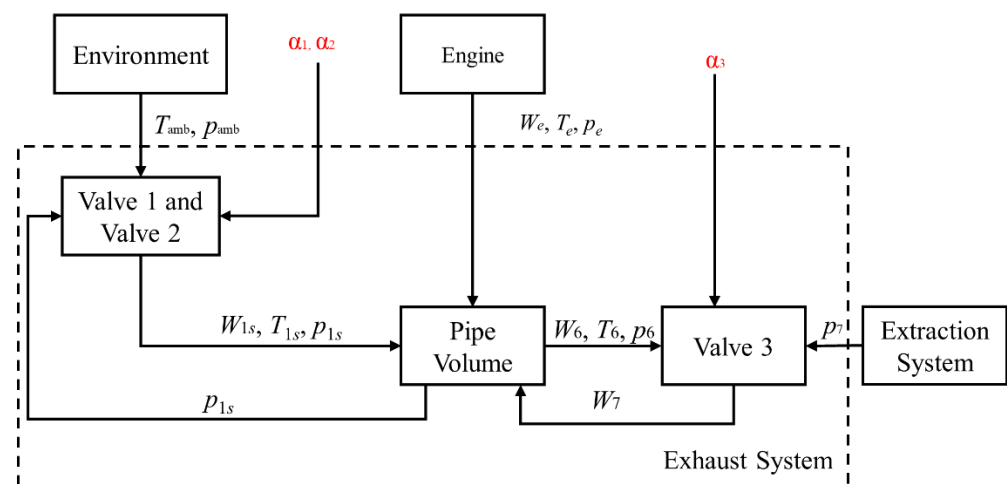


**Figure 20.** Logic diagram of exhaust system built with lumped parameters.

Therefore, to further verify the advantage of the exhaust system built with the multi-cavity iterative modeling method, it was compared with the traditional lumped-parameter model. The simulation was carried out under the same conditions shown in Figure 15. The simulation results are shown in Figure 21, where the experimental data are marked with a solid line, and the simulation results are marked with a dashed line.

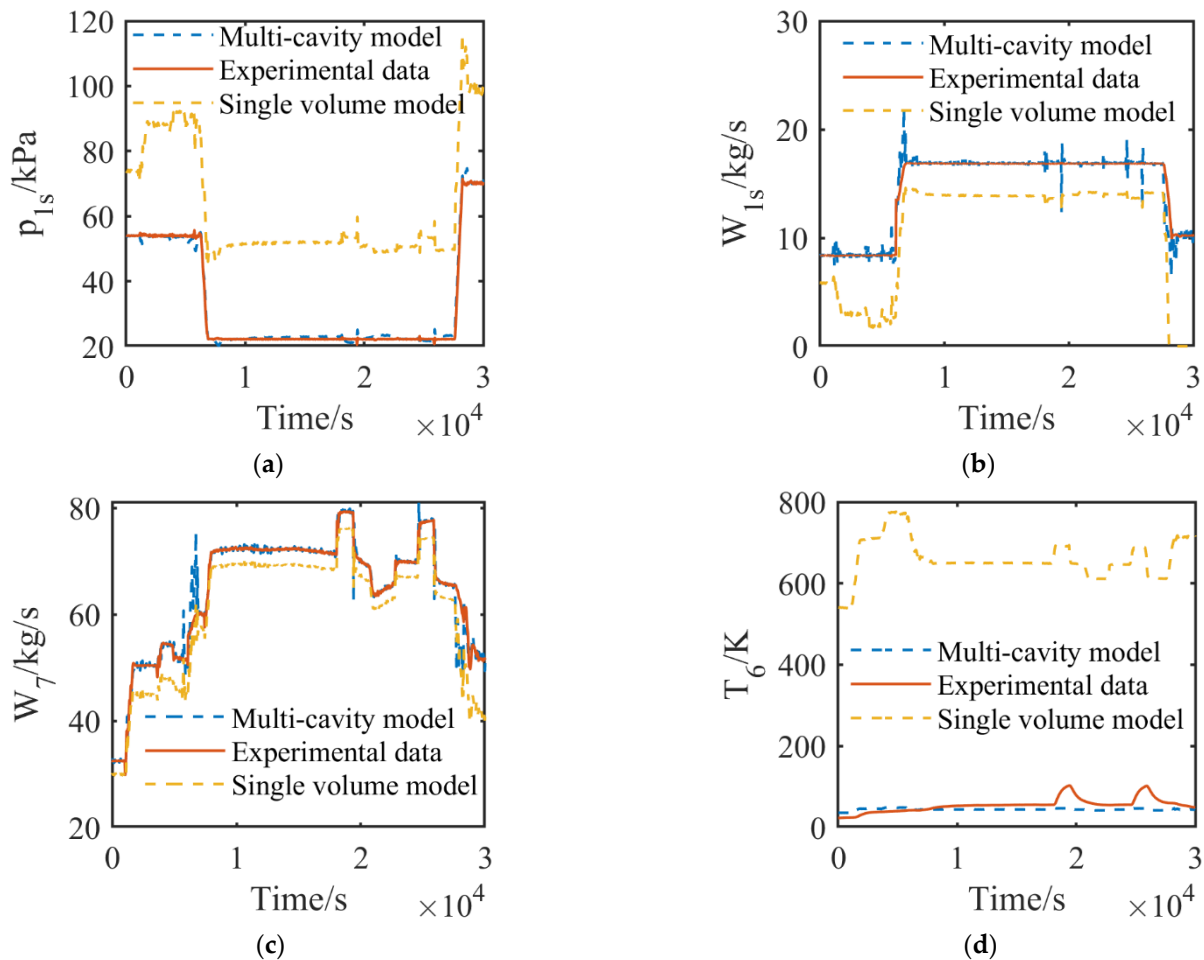


**Figure 21.** Parameter comparison between lumped-parameter model experimental data: (a) Pressure of exhaust system; (b) Valve flow of exhaust system; (c) Total flow of exhaust system; (d) Temperature before Valve 3.

It is shown in Figure 21a that the test chamber pressure obtained with the single-volume lumped-parameter model is much higher than that of the experimental data and the multi-cavity model simulation results. The secondary flow cannot be obtained with the single-volume model and is simplified as the valve flow. Due to the higher pressure in the test chamber, the valve flow  $W_v$  calculated with the single-volume model is smaller than that of the experimental data and the multi-cavity model simulation results. The difference between the experimental data and the multi-cavity model simulation results in Figure 21b was a result of replacing the experimental  $W_{1s}$  with  $W_v$ , because the secondary flow could not be measured directly in the experiment.

Moreover, the total mass flow of the exhaust system is shown in Figure 21c. The smaller total mass flow of the single-volume model results from the much higher temperature before Valve 3, because the lumped-parameter model does not consider the heat exchange in the cooler. The temperature before Valve 3 is shown in Figure 21d.

#### 4.3. Closed-Loop Simulation Results

To verify the performance of the exhaust system built with the multi-cavity method in a closed-loop system, the manual switch module was switched, and the control loop was activated, as shown in Figure 16.

The simulation results are shown in Figure 22. The pressure in the test chamber fits the experimental data, and the difference between  $\alpha_3$  is relatively small, which further verifies the accuracy of the exhaust system model. It proves that the exhaust system model can be used to design and test the control algorithm. Moreover, the response of the mass flow, shown in Figure 23, is similar to the mass flow response, shown in Figure 19, with a smaller mass flow fluctuation.

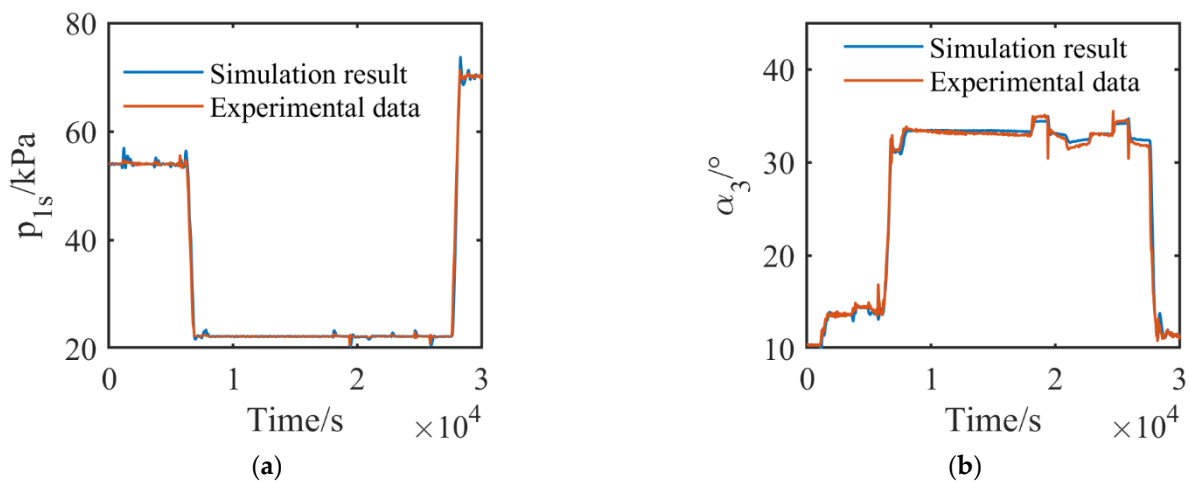


**Figure 22.** Comparison of closed-loop simulation results and experimental data: (a) Pressure of exhaust system; (b) Opening of Valve 3 in exhaust system.

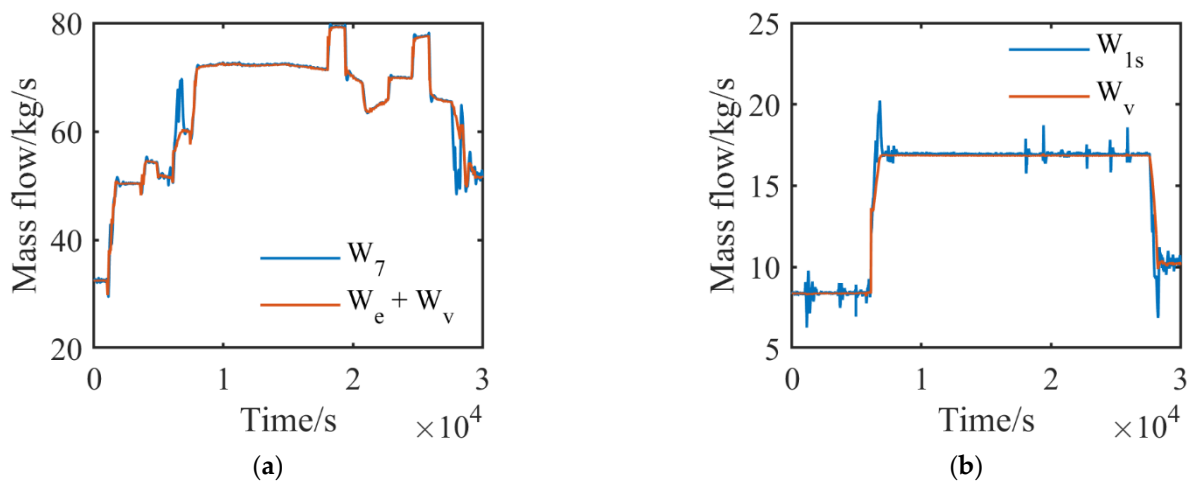


**Figure 23.** Closed-loop simulation results of mass flow: (a) Flow of exhaust system; (b) Flow of test chamber.

#### 5. Conclusions

A multi-cavity iterative modeling method is proposed, which aims at improving accuracy and reflects the dynamic process of the exhaust system model. The conclusions that were obtained are listed as follows:

1. The multi-cavity iterative model is able to simulate the pressure in the test chamber and in the exhaust system. The simulation results show that the maximum error of pressure in the test chamber is 2 kPa in the steady state and 5 kPa in the transient process compared with the experimental data. The pressure error in the exhaust system is no more than 2 kPa

in the steady state and no more than 6 kPa in the transient process compared with the experimental data.

2. The simulation results of the multi-cavity iterative model were compared with the lumped-parameter model under the same working conditions. This showed that the model built with the proposed method has advantages of calculating the pressure and mass in the exhaust system accurately over the lumped-parameter model.

3. The multi-cavity iterative model was tested in a closed-loop system. The results show that the pressure in the test chamber can be controlled to the desired value, and the opening of the valve is only slightly different from the experimental data, which further verifies the accuracy of the exhaust system model and proves the model's capability of being used to design and test the control algorithm.

Impurities such as water vapor should be considered in the future, because engine emissions have been a hot issue for decades, and new AGTFs that are able to carry out research on the icing and noxious gases of engines are being built. It increases the demand of the exhaust system model, and the modeling method should be improved to support the research.

**Author Contributions:** Conceptualization, K.M. and X.W. (Xi Wang); methodology, K.M. and X.W. (Xi Wang); software, K.M., M.Z. and J.L.; validation, K.M., S.Z., Z.D. and X.W. (Xin Wang); writing—original draft preparation, K.M.; writing—review and editing, K.M., M.Z., S.Y. and X.P.; visualization, K.M. and L.Z.; supervision, M.Z.; project administration, X.W. (Xi Wang). All authors have read and agreed to the published version of the manuscript.

**Funding:** This research was funded by the AECC Sichuan Gas Turbine Establishment Stable Support Project, grant number GJCZ-0011-19; the National Science, Technology Major Project, grant number 2017-V-0015-0067; and the Technology Major Project, grant number 2019-V-0010-0104.

**Data Availability Statement:** Not applicable.

**Conflicts of Interest:** The authors declare no conflict of interest.

## References

1. Hou, M.J. *Aero-Engine Altitude Simulating Test Techniques*; Aviation Industry Press: Beijing, China, 2014; p. 1.
2. Zhu, M. *Thermal Fluid Mechanism Analysis and the Research of Modern Control Methods for Altitude Ground Test Facilities*; Beihang University: Beijing, China, 2021.
3. Gerald, A.; Joseph, K. Numerical modeling of altitude diffusers. In Proceedings of the 19th Advanced Measurement and Ground Testing Technology Conference, New Orleans, LA, USA, 17–20 June 1996.
4. Li, G.; Zhang, J. *Aeronautic Ejector/Mixer*; National Defense Industry Press: Beijing, China, 2007; pp. 15–26.
5. Byung, H.; Jihwan, L.; Sunghyun, P.; Ji, H.; Woongsup, Y. Design and Analysis of a Second-Throat Exhaust Diffuser for Altitude Simulation. *J. Propuls. Power* **2012**, *28*, 1091–1104.
6. Montgomery, P.A.; Burdette, R.; Krupp, B. A Real-Time Turbine Engine Facility Model and Simulation for Test Operations Modernization and Integration. In Proceedings of the ASME Turbo Expo 2000: Power for Land Sea, and Air, Munich, Germany, 8–11 May 2000.
7. Montgomery, P.A.; Burdette, R.; Wilhite, L.; Salita, S. Modernization of a Turbine Engine Test Facility Utilizing a Real-Time Facility Model and Simulation. In Proceedings of the ASME Turbo Expo 2001: Power for Land Sea, and Air, New Orleans, LA, USA, 4–7 June 2001.
8. Davis, M.; Montgomery, P. A Flight Simulation Vision for Aeropropulsion Altitude Ground Test Facilities. In Proceedings of the ASME Turbo Expo 2002: Power for Land Sea, and Air, Amsterdam, The Netherlands, 3–6 June 2002.
9. Boraira, M.; Van Every, D. Design and Commissioning of a Multivariable Control System for a Gas Turbine Engine Test Facility. In Proceedings of the 25th AIAA Aerodynamic Measurement Technology and Ground Testing Conference, San Francisco, CA, USA, 5–8 June 2006.
10. Bierkamp, J.; Köcke, S.; Staudacher, S.; Fiola, R. Influence of ATF Dynamics and Controls on Jet Engine Performance. In Proceedings of the ASME Turbo Expo 2007: Power for Land Sea, and Air, Montreal, QC, Canada, 14–17 May 2007.
11. Weisser, M.; Bolk, S.; Staudacher, S. Hard-in-the-Loop-Simulation of a Feedforward Multivariable Controller for the Altitude Test Facility at the University of Stuttgart. 2013. Available online: <https://www.dglr.de/publikationen/2013/301179> (accessed on 9 February 2022).
12. Pei, X.T.; Zhang, S.; Dan, Z.H.; Zhu, M.Y.; Qian, Q.M.; Wang, X. Study on Digital Modeling and Simulation of Altitude Test Facility Flight Environment Simulation System. *J. Propul. Technol.* **2019**, *40*, 1144–1152.

13. Zhu, M.; Zhang, S.; Dan, Z.; Pei, X.; Wang, W.; Wang, X. A coordinate positioning and regression algorithm for the flow characteristics of a large butterfly valve. *Gas Turbine Exp. Res.* **2017**, *30*, 39–44.
14. Sosunov, V. The history of aviation engine development in the USSR and the 60th anniversary of CIAM. In Proceedings of the 26th Joint Propulsion Conference, Orlando, FL, USA, 16–18 July 1990.
15. Pei, X.; Liu, J.; Wang, X.; Zhu, M.; Zhang, L.; Dan, Z. Quasi-One-Dimensional Flow Modeling for Flight Environment Simulation System of Altitude Ground Test Facilities. *Processes* **2022**, *10*, 377. [[CrossRef](#)]
16. Sheeley, J.M.; Sells, D.A.; Bates, L.B. Experiences with Coupling Facility Control Systems with Control Volume Facility Models. In Proceedings of the 42nd AIAA Aerospace Sciences Meeting and Exhibit, Reno, NE, USA, 5–8 January 2004.
17. Zhu, M.; Wang, X.; Zhang, S.; Dan, Z.; Pei, X.; Miao, K.; Jiang, Z. PI Gain Scheduling Control for Flight Environment Simulation System of Altitude Ground Test Facilities Based on LMI Pole Assignment. *J. Propuls. Technol.* **2019**, *40*, 2587–2597.
18. Qian, Q.; Dan, Z.; Zhang, S.; Pei, X.; Wang, W. Linear active disturbance rejection control method for intake pressure control in aero-engine transient test. *J. Aerosp. Power* **2019**, *34*, 2271–2279.
19. Zhu, M.; Wang, X.; Dan, Z.; Zhang, S.; Pei, X. Two freedom linear parameter varying u synthesis control for flight environment testbed. *Chin. J. Aeronaut.* **2018**, *32*, 1204–1214. [[CrossRef](#)]
20. Pan, J.; Shan, P. *Fundamentals of Gasdynamics*; National Defense Industry Press: Beijing, China, 2011; pp. 87–95.